Polymer Chemistry

ROYAL SOCIETY OF CHEMISTRY

PAPER

View Article Online
View Journal | View Issue

Check for updates

Cite this: *Polym. Chem.*, 2025, **16**, 994

Shedding light on surfactant-free emulsion polymerization†

Erika Paola Fonseca Parra, Jean-Luc Six and Khalid Ferji *

Received 26th September 2024,
Accepted 21st January 2025

DOI: 10.1039/d4py01076k

rsc.li/polymers

Herein, we introduce a sustainable method for latex production *via* surfactant-free emulsion polymerization (SFEP) carrying out a photoinitiated polymerization (photo-SFEP) under both artificial light and sunlight. We discuss the use of sodium phenyl-2,4,6-trimethylbenzoylphosphinate (TPO-Na) as a water-soluble photoinitiator to *in situ* prepare polymeric nanoparticles under mild conditions, eliminating the need of conventional surfactants. The methodology exploits the rapid photolysis of TPO-Na, which generates anionic radical species that initiate the polymerization of glycidyl methacrylate (GlyMA), selected as a model monomer. Photo-SFEP was optimized to ensure colloidal stability over several months, even under varying environmental ionic strengths. The structural and colloidal properties of the nanoparticles were thoroughly characterized using dynamic light scattering (DLS), transmission electron microscopy (TEM), and zeta potential measurements, confirming the reproducibility and robustness of the latex dispersions. Our methodology shows promise as a scalable, efficient alternative to conventional emulsion polymerization techniques. Additionally, its versatility was affirmed by extending its application to various vinylic monomers, showcasing its broad potential.

1. Introduction

The term 'latex' refers to a colloidal dispersion of polymeric nanoparticles in water, stabilized by surfactants.[1] Emulsion polymerization, originally developed in the mid-20th century to mimic natural rubber latex,[2–4] involves polymerizing hydrophobic monomers in water stabilized by surfactants above their critical micelle concentration. However, the use of surfactants can introduce technical challenges. For instance, in the application of water-based paints, surfactants may migrate to the latex film-air interface after drying, compromising interfacial properties of the material.[5,6]

Significant efforts have been made over the past decades to prevent surfactant mobility by limiting their dynamic exchange behavior.[7] Strategies include covalently linking surfactants to core-forming nanoparticles, and chemically modifying surfactants to introduce reactive groups that act as initiators (inisurf),[8–10] monomers (surfmer),[11,12] or chain transfer agents (transurf)[13,14] in emulsion polymerization. However, issues like unfavourable reactivity ratios of monomers, loss of stability and poor size control of latex persist. A recent alternative involves generating macromolecular surfactants *in situ via* polymerization-induced self-assembly (PISA).[15–20] In emulsion PISA,[21] solvophobic monomers are polymerized from reactive solvophilic steric polymers, leading to *in situ* formation of amphiphilic copolymers that spontaneously self-assemble into monomer-swollen nano-objects. Subsequently, chain polymers continue to develop inside the core of nano-objects.

Another appropriate approach is the complete elimination of surfactants within the process, through surfactant-free emulsion polymerization (SFEP).[22–24] In principle, SFEP relies on incorporating charged groups at the polymer chain-ends, providing inter-particle electrostatic repulsion to enhance colloidal latex stability.[7] This is achieved *in situ* by polymerizing hydrophobic monomers in water with a water-soluble radical initiator, forming ionic radical fragments.[25–28] In their seminal work, R. H. Ottewill and coll.[29] formulated stable polystyrene latex without surfactants, relying on electrostatic repulsion of persulphate fragments produced by the thermal decomposition of potassium persulfate (KPS) initiator. They identified key conditions for successful SFEP: high temperatures to favor rapid radical generation, dilute latex dispersion, and high initiator/monomer ratios. We are considering whether these stringent conditions can be optimized to be more practical, scalable, and applicable for industrial use.

Over the past decades, light has been recognized as a cleaner and environmentally friendly energy source compared to thermal methods in chemistry,[30,31] and more specifically in polymer synthesis.[32,33] Light can be easily modulated and localized, enabling on-demand initiation and termination of

Université de Lorraine, CNRS, LCPM, F-54000 Nancy, France.
E-mail: khalid.ferji@univ-lorraine.fr

† Electronic supplementary information (ESI) available. See DOI: https://doi.org/10.1039/d4py01076k

polymerization reactions, resulting in control over polymerization kinetics and molecular weight distribution. In the literature, most studies on radical polymerization focus on thermal initiation,[34–38] which involves the homolysis of peroxide or azo compounds that generally require high activation energy at temperatures above 60 °C. In contrast, photolysis of photoinitiators (PIs) is temperature-independent, with low initial activation energy as the energy produced by the excitation of a chromophore exceeds that required for homolysis to generate primary radicals.[39,40] The high reactivity of PIs allows for the rapid generation of radicals, which we hypothesize could improve the efficiency of SFEP. Acylphosphine oxide derivatives have attracted significant attention in both academia and industry as PIs due to their strong light absorption and ability to rapidly generate highly reactive radicals.[41–47] While most PIs in this important class are organo-soluble, their direct application to SFEP can present challenges related to the heterogeneous reaction medium. This does not necessarily preclude their use, but rather highlights the need to adapt or modify PIs to achieve compatibility with aqueous systems.

The primary objective of the present study was to enhance the efficiency of SFEP strategy by utilizing light instead of heat for the radical initiation process. After evaluating various PIs, sodium phenyl-2,4,6-trimethylbenzoylphosphinate (TPO-Na, Fig. 1) emerged as the most suitable candidate, owing to its water solubility, rapid photolysis, and ability to generate ionic radical fragments. TPO-Na has been previously investigated as a PI to drive PISA in aqueous dispersions.[48–50] However, to the best of our knowledge, its potential application in SFEP has not yet been thoroughly explored or reported in the literature. Glycidyl methacrylate (GlyMA) was chosen as a model monomer to optimize the experimental conditions (Fig. 1). Our study demonstrates that TPO-Na can rapidly form and stabilize latex dispersions in a simple reaction medium, achieving colloidal stable latex up to 20% w/w solids content by using very low TPO-Na/monomer molar ratios (R), even in the presence of salts. In this study, the latex formulations are denoted as AS-RGlyMaSC, where 'AS' indicates the activation source (T for thermal polymerization at 60 °C, P for photopolymerization at 405 nm, and SL for sunlight), 'R' refers to the TPO-Na/GlyMA molar ratio expressed in ‰, and 'SC' represents the solids content expressed in w/w%.

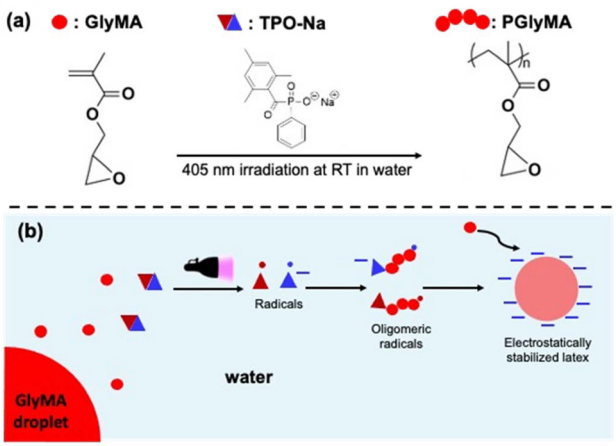

Fig. 1 (a) Synthesis pathway and (b) schematic illustration for the preparation of PGlyMA latex *via* photo-SFEP of GlyMA in the presence of TPO-Na photoinitiator.

2. Materials and methods

2.1. Chemicals and reagents

Glycidyl methacrylate (GlyMA, Merck, 97%), vinyl acetate (VAc, Merck, ≥99%), styrene (S, Merck, 99%), methyl methacrylate (MMA, Merck, 99%), *n*-butyl acrylate (BA, Merck, ≥99%), ethyl (2,4,6-trimethylbenzoyl) phenylphosphinate (TPO-L, Fluorochem), sodium bromide (NaBr, Merck, ≥99.99%), sodium chloride (NaCl, VWR Chemicals), *N*,*N*-dimethylformamide (DMF, Merck, ≥99.8%) and 2-butanone (Acros organics, 99%), potassium persulfate (KPS, Merck, ≥99%), Alcian blue (Merck) were used as received.

2.2. Synthesis of water-soluble photoinitiator TPO-Na

TPO-Na was prepared *via* chemical modification of TPO-L (Scheme S1†) as previously reported in the literature.[51] In a 100 mL round-bottom flask, TPO-L (5 g, 15.8 mmol) and NaBr (1.75 g, 17 mmol) were added under nitrogen to 2-butanone (50 mL) and the reaction mixture was stirred overnight at 50 °C in the dark. The white precipitate formed was recovered by filtration, washed three times with 2-butanone, dried overnight under reduced pressure at 50 °C, and then analyzed by ^{1}H NMR (Fig. S1†).

2.3. Photoinitiated surfactant-free emulsion polymerization (photo-SFEP) of GlyMA at room temperature

The experimental conditions used for all formulations are summarized in Table S1.† All experiments were conducted at ambient temperature (RT), which varied between 20 and 25 °C, as photopolymerization is not significantly influenced by such temperature deviations. In a typical experiment targeting a solids content (SC%) of 10% w/w and R = (n_{TPO-Na}/n_{GlyMA}) × 1000 = 1‰: into 20 mL dried glass vial, 700 μL of GlyMA (0.7 g, 4.9 mmol) were dispersed in 6.1 mL of distilled water (pH ~ 6.5). 20 μL of DMF were added as an internal standard for ^{1}H NMR analysis. A stirrer magnetic bar was added, and the glass vial was sealed with a septum prior to deoxygenation by nitrogen bubbling for 10 min. 159 μL (1.6 mg, 4.9 μmol) of a separately degassed stock solution of TPO-Na in water (10 mg mL^{-1}) were transferred to the reaction medium under nitrogen. Subsequently, the heterogeneous mixture was irradiated at 405 nm (30 mW) using a light source (Opto-Spectrum Generator L12194-00-39-070) or sunlight, as shown in Fig. S2† and Fig. 6b respectively. After less than 30 min of irradiation, the crude white latex was analyzed by ^{1}H NMR to evaluate the monomer conversion (Fig. S3†).

2.4. Photo-SFEP of GlyMA at 60 °C

Experiments were performed according to the experimental protocol described above (section 2.3) but at 60 °C instead of RT.

2.5. Surfactant-free emulsion polymerization of GlyMA at 60 °C

Experiments were performed according to the experimental protocol described above (section 2.3) in dark at 60 °C and in the presence of KPS instead of TPO-Na.

2.6. Photo-SFEP of GlyMA at large scale

In a 1.5 L homemade glass photoreactor, 188 mL of GlyMA (202 g, 1.4 mol) were dispersed in 805 mL of distilled water, and 2 mL of DMF were added as an internal standard for NMR analysis. Once the reactor was sealed, the mixture was stirred using a propeller agitator (500 rpm, BIOLOCK SCIENTIFIC), and deoxygenation was performed by nitrogen bubbling for 30 minutes. Then, 4.6 mL (0.4 g, 1.4 mmol) of a degassed stock solution of TPO-Na in water (100 mg mL^{-1}) were transferred into the reaction medium under nitrogen. Subsequently, the heterogeneous mixture was irradiated. After 1 hour of irradiation, the crude white latex obtained was analysed by ^{1}H NMR to assess the monomer conversion.

2.7. Characterization methods

2.7.1. ^{1}H NMR spectroscopy. ^{1}H NMR analysis was conducted on a Bruker Avance 300 MHz NMR spectrometer in DMSO-d_6.

2.7.2. Size exclusion chromatography. Prior to SEC analysis, the samples underwent pre-treatment to neutralize the surface charges of the nanoparticles. This pre-treatment involved five cycles where 200 µL of the particle dispersion was added to 800 µL of distilled water and 20 µL of 1 M HCl. After each addition, the mixture was centrifuged for 1 minute, and the excess liquid was carefully removed. The resulting precipitate was lyophilized and dissolved in THF at a concentration of 10 mg mL^{-1}. The molecular weights of the nanoparticles were determined using a SEC system operating in THF at a flow rate of 1 mL min^{-1} and a temperature of 25 °C. The system was equipped with a multi-angle laser light scattering (MALLS) detector (miniDawn Wyatt), a differential refractometer detector (RID-10A, Shimadzu), an HPLC pump (LC-20AD, Shimadzu), a degasser (DGU-20A3R, Shimadzu), and three PLgel columns with pore sizes of 100 000 Å, 1000 Å, and 100 Å.

2.7.3. Dynamic light scattering. The hydrodynamic diameter (D_h) and size distribution (PDI) of nano-objects were determined at 20 °C using an ALV/CGS-3 compact goniometer system equipped with an ALV7004 multiple tau digital correlator and a vertically polarized He–Ne laser of 22 mW output power operating at wavelength λ = 632.8 nm. The autocorrelation functions were analyzed in terms of relaxation time (τ) distribution according to the REPES routine.[52] Measurements were done at different angles θ, which varied from 20 to 150°, corresponding to scattering wave vectors q ranging from q = 4.6×10^{-3} to 2.55×10^{-2} nm^{-1}. D_h was estimated using the Stokes–Einstein relation (1), where D_0 is the diffusion coefficient, k_B is the Boltzmann constant, T is the experimental temperature (293 K), and η_s is the viscosity of water.

$$D_h = \frac{k_B T}{3\pi\eta_s D_0} \quad (1)$$

2.7.4. Transmission electron microscopy. Prior to sample deposition, the carbon-coated grids were treated with Alcian blue, which was used both for negative staining and to facilitate adhesion of the negatively charged nanoparticles. Specifically, the grids were first exposed to a drop of Alcian blue solution for 1 minute, followed by gentle washing with a drop of distilled water. Ten microliters of the nano-object suspension were then placed on the treated grids and left for 2 minutes to allow proper adsorption. Excess liquid was carefully blotted. The grids were subsequently visualized at 5.5 kV using a LVEM5 Benchtop Electron Microscope (Delong Instruments). The TEM diameter (D_{TEM}) corresponds to the average of at least 50 nanoparticle diameters using ImageJ software.

2.7.5. Zeta potential. The zeta potential (ζ) values were determined at 20 °C using a Zetasizer nano series of Malvern instruments. Each value corresponds to the average of 3 runs of the analyzer.

3. Results and discussion

3.1. TPO-Na: synthesis and photophysical properties

TPO-Na is easily synthesized in a single step[51] (Scheme S1†) from the commercially available Ethyl (2,4,6-trimethylbenzoyl) phenylphosphinate (TPO-L).[53–55] Fig. S1† shows the ^{1}H NMR spectra for both TPO-L and TPO-Na, confirming the successful synthesis of TPO-Na. The disappearance of the methyl and methylene protons (f and g) in the spectrum of TPO-Na, which are previously present in the spectrum of TPO-L, indicates the quantitative synthesis of TPO-Na. On the other hand, the modification of TPO-L to TPO-Na induces a noticeable change in the UV absorption spectrum, particularly in the region between 320–370 nm. DMSO was used as a common solvent for both TPO-Na and TPO-L, allowing for a more direct comparison of their absorption spectra in a non-aqueous medium. As shown in Fig. S4,† TPO-Na in water exhibits a slight blue shift in comparison to TPO-Na and TPO-L in DMSO. Beyond the region around 370 nm, no significant changes are observed between the spectra.

3.2. Photo-SFEP *versus* thermal-SFEP

To compare the performance of photoinitiation *versus* thermal-initiation, we reproduced the requested experiment conditions suggested by R. H. Ottewill and coll.,[29] using GlyMA as model monomer and KPS as thermal initiator. All experiments were conducted using distilled water (pH ~ 6.5) to prevent the hydrolysis of the epoxy group of GlyMA moities.[56] Their experiment, carried out at 60 °C in a dilute

medium (SC = 2.2% w/w) with a high initiator-to-monomer ratio (R = 20‰), required over 2 hours to achieve high monomer conversion. Spherical nanoparticles with a diameter estimated by TEM (D_{TEM}) of 118 nm were produced (Fig. 2a). Additional TEM images are provided in the ESI (Fig. S5†). However, dynamic light scattering (DLS) indicated much larger hydrodynamic diameters (D_h = 977 nm), suggesting significant particle aggregation. This apparent size disparity between D_h and D_{TEM} can be attributed to the aggregation behaviour in the dispersion. Such aggregation leads to an increased apparent size in DLS measurements, which record the motion of particle clusters rather than individual nanoparticles. Precipitation occurring after a few hours further supports the occurrence of aggregation of the particles (Fig. 2b).

Photoinitiated SFEP (photo-SFEP) using TPO-Na under 405 nm irradiation at room temperature (RT) was performed to evaluate the impact of photoinitiation on nanoparticle stability. The use of 405 nm visible light reduces light scattering compared to shorter UV wavelengths, enabling effective penetration in the aqueous reaction medium. Additionally, the high solubility of TPO-Na in the continuous phase ensures uniform initiation. Complete monomer conversion occurred in less than 30 minutes when TPO-Na was used instead of KPS. In comparison with previous experiment, Fig. 2c shows the formation of nanoparticles with smaller hydrodynamic and TEM diameters. Negative zeta potentials were observed in both cases. Note that TEM images revealed nanoparticles appearing connected, likely due to water pulling them together through capillary action during TEM-grid drying. High-resolution TEM confirms this behaviour (Fig. S6†). Importantly, the nanoparticle dispersion remained stable for at least three months (Fig. 2d), indicating that TPO-Na is an effective photoinitiator for surfactant-free latex formulations. A similar synthesis using photo-SFEP conducted at 60 °C resulted in the production of stable latex nanoparticles of similar diameters to those obtained at RT (Fig. S7a†), indicating that temperature does not significantly affect the final product.

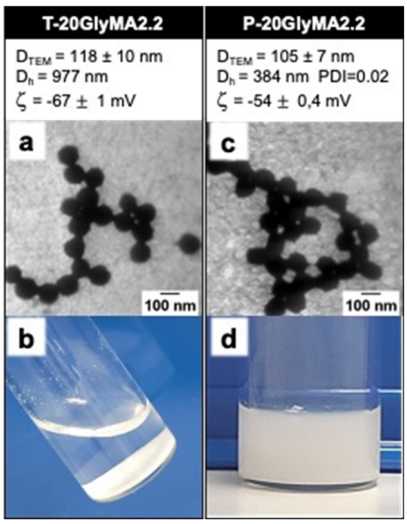

Fig. 2 Surfactant-free latex prepared *via* SFEP of GlyMA at 60 °C (T-20GlyMA2.2) and under 405 nm irradiation at RT (P-20GlyMA2.2) using R = 20‰ and SC = 2.2% w/w in water. (a and c) TEM images of latex immediately after synthesis. (b and d) Photographs of latex dispersions after three months in dark at RT.

To further investigate the origin of this stability, a similar synthesis was performed using TPO-L, the oil-soluble precursor of TPO-Na. In this case, only precipitation was observed (Fig. S8†), demonstrating that the ionic charges introduced by TPO-Na play a critical role in stabilizing the latex dispersions through electrostatic repulsion.

3.3. Effect of TPO-Na/GlyMA molar ratio

We addressed the challenge of minimizing the amount of TPO-Na photoinitiator employed during SFEP while ensuring the stability and desired properties of the resulting latex particles. Consequently, the TPO-Na/GlyMA molar ratio (R) was progressively reduced to 0.08‰. All experiments were performed at SC of 10% w/w. Furthermore, analysis of the produced polymeric chains by SEC revealed bimodal and broad chromatograms, with dispersities exceeding 1.5 (Fig. S9 and S10†). This behaviour is expected due to the conventional radical polymerization mechanism employed in this work, where chain length control is inherently absent. It is important to note that controlling the polymer chains was not an objective of this study.

Colloidal stability was tracked using DLS, TEM and zeta potential (ζ) for three months (Fig. 3). Additional TEM images are provided in the ESI (Fig. S11–S16†). Immediately after formulation, varying the ratio TPO-Na/GlyMA from 2.5‰ to 0.5‰ did not significantly affect the polymerization rate (complete conversion after less than 1 h of irradiation), nor did influence the physical characteristics of latex, as D_h, D_{TEM} and ζ remain low and relatively constants (Fig. 3). All R ratios in this range lead to suspension with great stability for at least three months. Further reducing the R ratio below the threshold value of R = 0.5‰ resulted in a gradual increase in D_h, leading to a rapid precipitation at R = 0.08‰. This highlights the critical role of maintaining a sufficient PI concentration to ensure effective polymerization and prevent particle aggregation. Our results demonstrate that at SC = 10%, the concentration of TPO-Na in photo-SFEP for ensuring stable latex dispersions could be reduced to 0.5‰. Below this ratio, there is insufficient PIs to generate enough anionic radicals for initiating the polymerization and subsequently stabilizing the dispersion by electrostatic repulsions. Note that latex synthesis *via* SFEP conducted at 60 °C in the presence of low KPS/GlyMA molar ratio (R = 1‰) resulted in a direct precipitation (Fig. S7b†), confirming the limitation of persulphate in latex stabilization at low R.

3.4. Effect of the solids content

Solids content (SC) is a critical parameter to consider when developing any novel latex formulation methodology. To evaluate the ability of photo-SFEP to produce more concentrated dispersion, latex was prepared with SC values ranging from 2.2% w/w to 50% w/w, while maintaining a constant TPO-Na/GlyMA ratio of 1‰. Experiments conducted at SC equal to

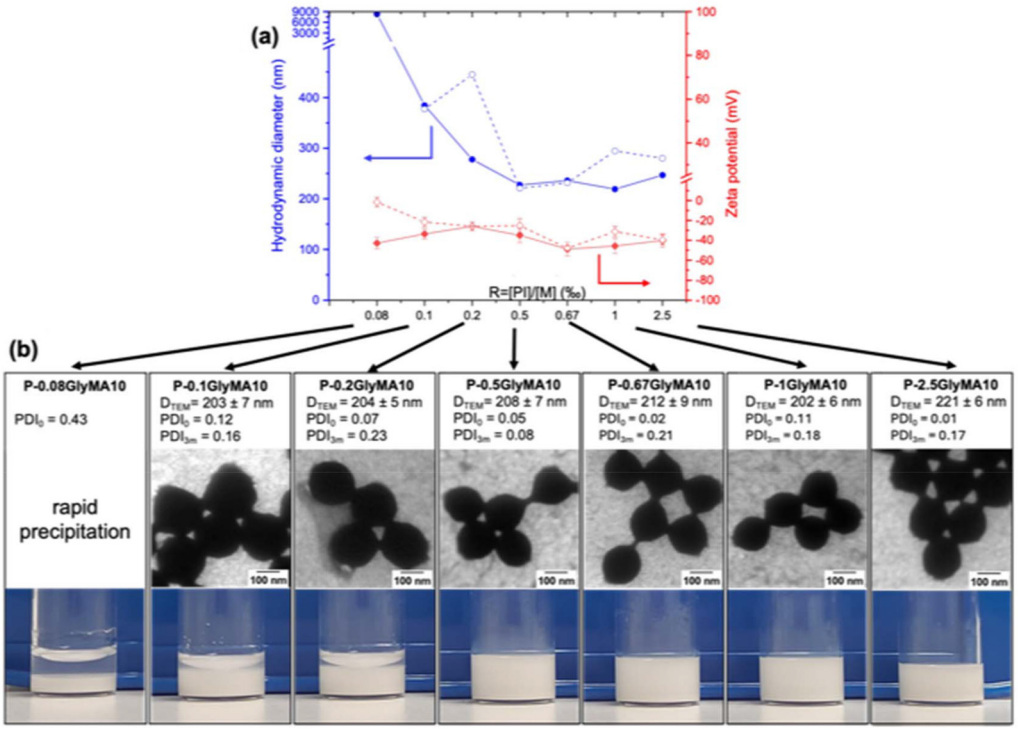

Fig. 3 Surfactant-free latex prepared *via* photo-SFEP of GlyMA under 405 nm irradiation at SC = 10% w/w in water, at RT and using different TPO-Na/GlyMA molar ratios. (a) Hydrodynamic diameters (circle) and zeta potentials (diamond) of nanoparticles immediately after formulation (open symbols) and after three months (solid symbols). (b) TEM images of nanoparticles immediately after formulation, and photographs of latex dispersions after three months. D_{TEM} values represent the average diameter of at least 50 nanoparticles, measured using ImageJ software. PDI values were obtained from DLS measurements at a 90° angle, recorded immediately after formulation (PDI_0) and after 3 months (PDI_{3m}).

30%, 40%, and 50% w/w produced unstable latex dispersions (Fig. S17†). In contrast, latex synthesized at SC below 20% w/w (Fig. 4) displayed similarly low zeta potentials, with a dependency of nanoparticle size on SC. Specifically, increasing SC led to a corresponding increase in both D_h and D_{TEM} of the nanoparticles. Additional TEM images are provided in the ESI (Fig. S18 and S19†). After three months, the zeta potentials remained relatively stable, indicating excellent colloidal stability, as also observed in the latex dispersion images.

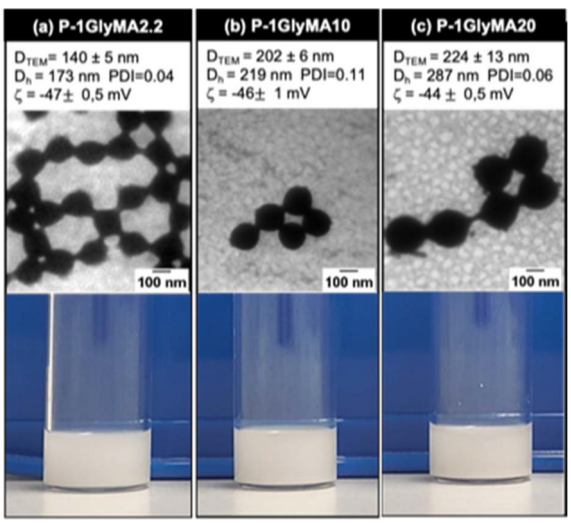

Fig. 4 Surfactant-free latex prepared *via* photo-SFEP of GlyMA under 405 nm irradiation using R = 1‰ at solids content of (a) 2.2% w/w, (b) 10% w/w and (c) 20% w/w.

3.5. Colloidal stability in ionic environment

One of the well-known challenges of SFEP is the destabilization of latex formulations in the presence of electrolytes.[29] In this context, our study seeks to assess the colloidal stability of latex produced *via* photo-SFEP, formulated with different ratios of TPO-Na and subsequently exposed to saline environments. Samples, initially prepared at a SC of 10% w/w, were diluted to 0.1% w/w using aqueous brine solutions with NaCl concentrations ranging from 10^{-4} mol L^{-1} to 1 mol L^{-1}. The colloidal stability of these nanoparticles was systematically monitored at two distinct time intervals: 2 hours and 3 months post-preparation. As shown in Fig. 5, all formulations exhibit consistent D_h up to a [NaCl] = 0.01 mol L^{-1}. However, the zeta potential values demonstrate a progressive increase with the salt concentration, indicating the progressive screening of the surface nanoparticles charge. Above a threshold [NaCl] of 0.01 mol L^{-1}, the formulations show marked signs of instability, highlighted by the increase of particles diameter and zeta potentials, especially when high TPO-Na/GlyMA molar ratio (R = 2.5‰) was used. This trend points to the aggregation and subsequent precipitation after

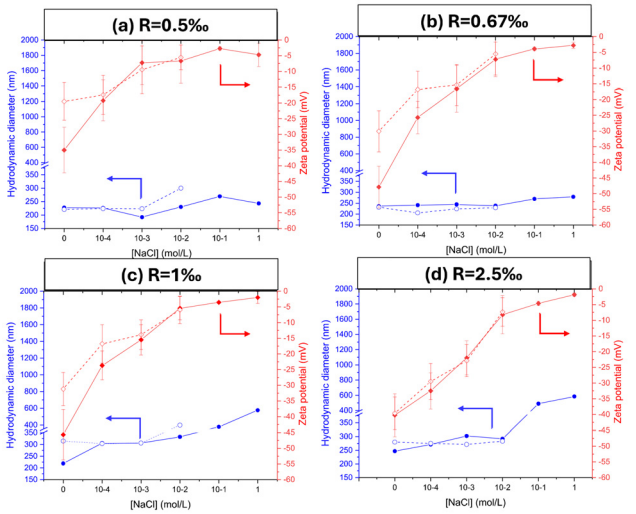

Fig. 5 Colloidal stability against salts of surfactant-free latex prepared *via* photo-SFEP of GlyMA under 405 nm irradiation in water at SC = 10% and differents *R* (a) 0.5‰, (b) 0.67‰, (c) 1‰ and (d) 2.5‰. Hydrodynamic diameter (circle) and zeta potential (diamond) of nanoparticles after 2 h (open symbols) and three months (solid symbols) of preparation.

three months as evidenced in the Fig. S20.† These findings illustrate that latex synthesized *via* photo-SFEP using TPO-Na exhibit good stability up to a brine concentration of 0.01 mol L^{-1} (Fig. S21†), which approximates the average ionic strength encountered in tap water. Similar observations were made during photo-SFEP in the presence of salts, where increasing the ionic strength above 0.01 g L^{-1} resulted in destabilization and particle aggregation (Fig. S22†).

3.6. Photo-SFEP sustainability

In line with the goal of developing more sustainable approaches to SFEP, we firstly investigated the lyophilization of latex and its subsequent re-dispersion in water. Lyophilization offers significant sustainability benefits enabling easier transportation, longer shelf-life, and reduced need for refrigeration or bulky liquid storage. Latex produced *via* photo-SFEP can be successfully lyophilized and re-dispersed with minimal impact on its colloidal stability and particle size distribution. Specifically, zeta potential of nanoparticles remained consistent after re-dispersion, highlighting the resilience of the colloidal system. Fig. 6a shows latex prepared at TPO-Na/GlyMA ratio of 0.67‰, then lyophilized and re-dispersed. TEM images further confirm that the morphological integrity of the latex particles is preserved after the drying and rehydration process. Similar results were observed for other ratios (Fig. S23–S26†). However, it is noted that the D_h increases from 231 nm to 376 nm upon redispersion, suggesting some degree of particle aggregation. This is attributed to the drying process, where particle interactions in the absence of stabilizers can lead to partial aggregation. Despite this, the system retains colloidal stability, demonstrating a relatively high degree of redispersibility.

Furthermore, we explored the potential of using sunlight as a direct energy source to carry out the photoinitiated polymerization, eliminating the need of artificial light source, and further enhancing the eco-friendliness of the process. We compared latex synthesized under sunlight (SL-1GlyMA10, Fig. 6b) with those prepared using artificial 405 nm irradiation (P-1GlyMA10, Fig. 4b). Both methods yielded stable dispersions after less than one hour of irradiation with similar diameters and zeta potentials, demonstrating that sunlight is an

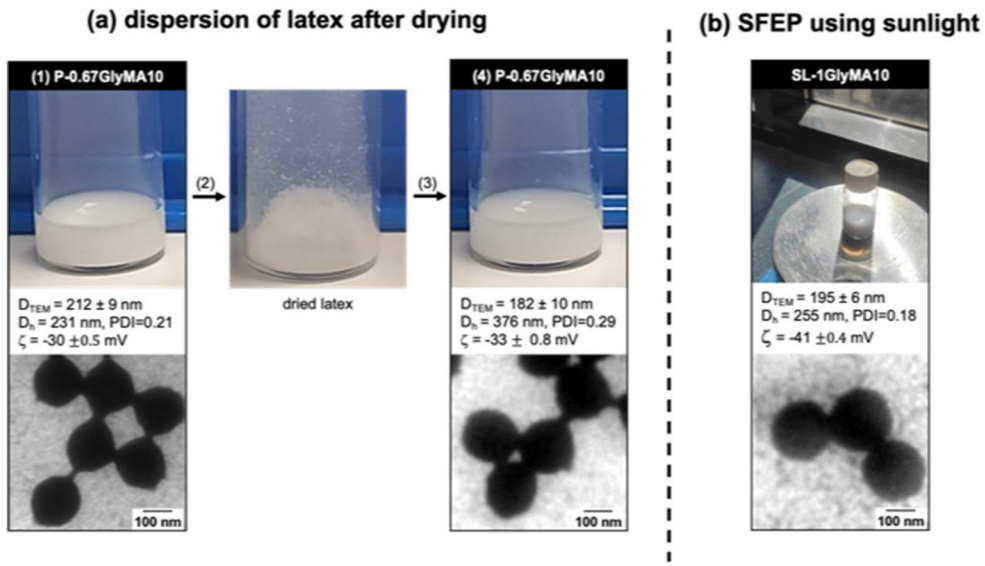

Fig. 6 Sustainability of photo-SFEP process. (a) (1) Surfactant-free latex prepared *via* photo-SFEP of GlyMA under 405 nm irradiation using *R* = 0.67‰ at SC = 10 w/w. (2) The nanoparticles were lyophilized and subsequently (3) re-dispersed in water targeting initial SC = 10 w/w. (b) Surfactant-free latex prepared *via* photo-SFEP of GlyMA under sunlight using *R* = 1‰ at SC = 10 w/w in water.

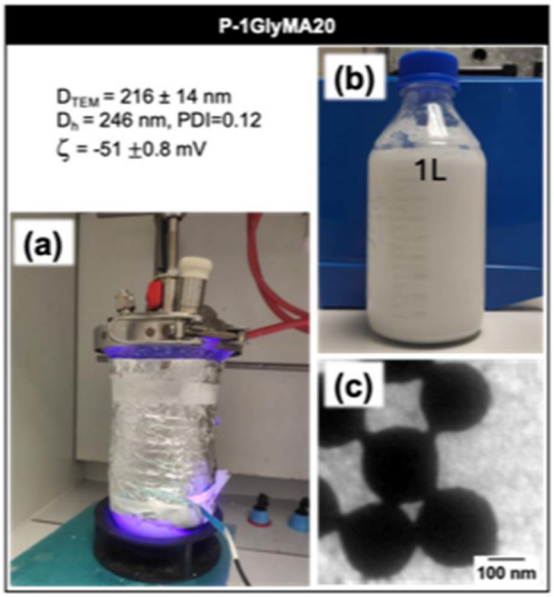

Fig. 7 Scale-up of surfactant-free latex synthesis *via* photo-SFEP of GlyMA under 405 nm irradiation. (a) Reaction setup for the scale-up to 1 liter, using R = 1‰ and SC = 20% w/w. (b) The resulting stable latex dispersion produced in a 1 L batch. (c) TEM image of nanoparticles in the latex.

effective and sustainable alternative for driving photo-SFEP. Additional TEM images are available in the ESI (Fig. S27†).

3.7. Photo-SFEP at large scale

To demonstrate the scalability of our photo-SFEP process, we successfully increased the reaction volume from 7 mL to 1000 mL, while maintaining both nanoparticle size and colloidal stability. Fig. 7a shows the setup for the scaled-up reaction, carried out under 405 nm irradiation, yielding a stable 1-liter latex dispersion (Fig. 7b).

The hydrodynamic diameter, polydispersity index, and zeta potential of the nanoparticles were measured after synthesis, with values of D_h = 246 nm, PDI = 0.12, and $\zeta = -51 \pm 0.8$ mV. These results are comparable to those obtained at smaller volumes (Fig. 4b), demonstrating that the scale-up of the process did not compromise the quality of the latex. TEM analysis (Fig. 7c and Fig. S28†) confirmed that the nanoparticles maintained their spherical morphology, with an average diameter of 216 ± 14 nm. Although some optimization is required, particularly regarding stirring rates to ensure uniform mixing in larger volumes, this experiment serves as a proof of concept for the scalability of the photo-SFEP process. It demonstrates the robustness of the method, allowing for larger volume production while preserving the desired particle properties and colloidal stability.

3.8. Photo-SFEP versatility

The versatility of the photo-SFEP process was assessed by exploring different hydrophobic monomer families, including vinyl acetate (VAc), methyl methacrylate (MMA), styrene (S), and *n*-butyl acrylate (BA). Photo-SFEP was conducted in distilled water with a R ratio of 1‰ and a SC of 10%. Full monomer conversion was obtained after less than one hour of irradiation at 405 nm, demonstrating the robustness of this approach across a wide range of monomers.

On one hand, as shown in Fig. 8, photo-SFEP of Vac, MMA and S resulted in the formation of spherical nanoparticles, with suspensions remaining stable for several months. While DLS measurements confirmed consistent size distributions for

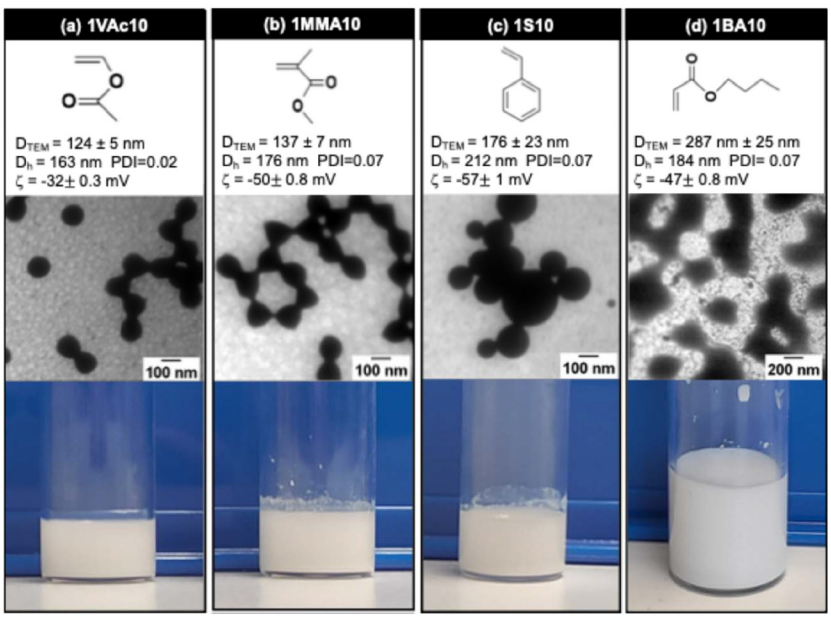

Fig. 8 TEM images and photographs of surfactant-free latex dispersions prepared *via* photo-SFEP under 405 nm irradiation at R = 1‰ and SC = 10% w/w of various monomers: (a) vinyl acetate (VAc), (b) methyl methacrylate (MMA), (c) and styrene (S), and (d) *n*-butyl acrylate (BA).

most of the monomers, TEM images revealed some deviation in particle size for S, where a broader particle distribution was observed (Fig. S29 and S31†). This indicates slight irregularities in particle size control for styrene, despite overall successful polymerization. Interestingly, compared to GlyMA, which produced larger nanoparticles (D_{TEM} = 202 nm, and D_h = 219 nm), Vac, MMA and S monomers yielded smaller nanoparticles. However, we do not yet have a rational explanation for the reduced particle sizes observed with these monomers. Further investigation will be required to fully understand the underlying mechanisms driving this size reduction.

On the other hand, experiments conducted with BA successfully produced nanoparticle dispersions, as confirmed by DLS measurements. However, obtaining clear TEM images proved challenging due to the low glass transition temperature (T_g) of poly(*n*-butyl acrylate), around −45 °C,[57] which caused deformation of the nanoparticles and hindered their visualization under electron microscopy at RT. Despite this limitation, the DLS data confirm successful polymerization and stable nanoparticle formation.

4. Conclusions

The present paper offers fresh insights into surfactant-free latex synthesis by utilizing light-driven surfactant-free emulsion polymerization, leading to an enhanced quality of the final latex. Using TPO-Na as a photoinitiator allowed us to conduct the process efficiently at relatively high solids content and with a minimal environmental impact. The study highlights the critical role of photoinitiator concentration and solids content in optimizing the stability and properties of the latex. Remarkably, we were able to use sunlight as energy source, which underscores the sustainability of our process. Additionally, the successful scale-up to 1 L demonstrated the robustness of this approach, showing that it remains effective even in larger volumes. We also demonstrated that the latex could be dried and successfully re-dispersed, potentially reducing transportation and handling costs significantly.

Further work is currently in progress to investigate the kinetics of photo-SFEP, with the goal of gaining a deeper understanding of the reaction mechanism underlying this methodology. Additionally, we have demonstrated the high efficiency of TPO-Na, even at very low concentrations, in the formulation of nanoparticles. This opens further avenues of research to investigate its influence on nanoparticle morphology when used as a photoinitiator instead of TPO-L[58,59] in PISA for instance. This approach not only adheres to sustainable practices but also advances the field of polymer chemistry, offering promising implications for industrial production.

Author contributions

Erika Paola Fonseca PARRA performed the experiments and wrote the first draft of the manuscript. Jean-Luc SIX supervised the work and revised the manuscript. Khalid FERJI conceptualized and designed the project, supervised the work, and wrote the final manuscript.

Data availability

The data supporting the findings of this study are fully included in the ESI† provided with this article. This includes all datasets, detailed methodologies, and analysis scripts necessary to reproduce the results.

Conflicts of interest

There are no conflicts to declare.

Acknowledgements

The present work has benefited from the platform APPEL of LCPM for NMR and DLS analyses. The authors acknowledge Ana Andrea Arteni from I2BC for high TEM resolution.

References

1 H. Kawaguchi, *Prog. Polym. Sci.*, 2000, **25**, 1171–1210.
2 W. V. Smith and R. H. Ewart, *J. Chem. Phys.*, 1948, **16**, 592–599.
3 G. S. Whitby and M. Katz, *Ind. Eng. Chem.*, 1933, **25**, 1338–1348.
4 W. D. Harkins, *J. Am. Chem. Soc.*, 1947, **69**, 1428–1444.
5 A. Guyot, *Adv. Colloid Interface Sci.*, 2004, **108–109**, 3–22.
6 P. A. Lovell and F. J. Schork, *Biomacromolecules*, 2020, **21**, 4396–4441.
7 C. Pichot, B. Charleux, M.-T. Charreyre and J. Revilla, *Macromol. Symp.*, 1994, **88**, 71–87.
8 S. S. Ivanchev, V. N. Pavljuchenko and N. A. Byrdina, *J. Polym. Sci., Part A: Polym. Chem.*, 1987, **25**, 47–62.
9 J. M. H. Kusters, D. H. Napper, R. G. Gilbert and A. L. German, *Macromolecules*, 1992, **25**, 7043–7050.
10 M. Wu, L. M. F. Ramirez, A. R. Lozano, D. Quemener, J. Babin, A. Durand, E. Marie, J. L. Six and C. Nouvel, *Carbohydr. Polym.*, 2015, **130**, 141–148.
11 A. Guyot and K. Tauer, *Polym. Synth.*, 2005, 43–65.
12 H. A. S. Schoonbrood and J. M. Asua, *Macromolecules*, 1997, **30**, 6034–6041.
13 T. S. Wilkinson, A. Boonstra, A. Montoya-Goñi, S. van Es, M. J. Monteiro and A. L. German, *J. Colloid Interface Sci.*, 2001, **237**, 21–27.
14 L. M. Forero Ramirez, J. Babin, A. Boudier, C. Gaucher, M. Schmutz, M. Er-Rafik, A. Durand, J.-L. Six and C. Nouvel, *Carbohydr. Polym.*, 2019, **224**, 115153.
15 N. J. W. Penfold, J. Yeow, C. Boyer and S. P. Armes, *ACS Macro Lett.*, 2019, **8**, 1029–1054.

16 D. Ikkene, J.-L. Six and K. Ferji, *Eur. Polym. J.*, 2023, **188**, 111848.
17 C. Liu, C.-Y. Hong and C.-Y. Pan, *Polym. Chem.*, 2020, **11**, 3673–3689.
18 F. D'Agosto, J. Rieger and M. Lansalot, *Angew. Chem., Int. Ed.*, 2020, **59**, 8368–8392.
19 J. L. Six and K. Ferji, *Polym. Chem.*, 2019, **10**, 45–53.
20 J. Yeow and C. Boyer, *Adv. Sci.*, 2017, **4**, 1700137.
21 B. Charleux, G. Delaittre, J. Rieger and F. D'Agosto, *Macromolecules*, 2012, **45**, 6753–6765.
22 P. J. Feeney, D. H. Napper and R. G. Gilbert, *Macromolecules*, 1987, **20**, 2922–2930.
23 S. T. Camli, F. Buyukserin, O. Balci and G. G. Budak, *J. Colloid Interface Sci.*, 2010, **344**, 528–532.
24 Q. Cao, T. Heil, B. Kumru, M. Antonietti and B. Schmidt, *Polym. Chem.*, 2019, **10**, 5315–5323.
25 F. A. Bovey and I. M. Kolthoff, *J. Polym. Sci.*, 1950, **5**, 487–504.
26 J. W. Goodwin, J. Hearn, C. C. Ho and R. H. Ottewill, *Br. Polym. J.*, 1973, **5**, 347–362.
27 A. Dunn and L. H. Chong, *Br. Polym. J.*, 1970, **2**, 49–59.
28 F. Stoffelbach, L. Tibiletti, J. Rieger and B. Charleux, *Macromolecules*, 2008, **41**, 7850–7856.
29 J. W. Goodwin, J. Hearn, C. C. Ho and R. H. Ottewill, *Colloid Polym. Sci.*, 1974, **252**, 464–471.
30 C. K. Prier, D. A. Rankic and D. W. C. MacMillan, *Chem. Rev.*, 2013, **113**, 5322–5363.
31 D. Staveness, I. Bosque and C. R. J. Stephenson, *Acc. Chem. Res.*, 2016, **49**, 2295–2306.
32 S. C. Ligon, B. Husar, H. Wutzel, R. Holman and R. Liska, *Chem. Rev.*, 2014, **114**, 557–589.
33 M. Chen, M. J. Zhong and J. A. Johnson, *Chem. Rev.*, 2016, **116**, 10167–10211.
34 K. Matyjaszewski and J. H. Xia, *Chem. Rev.*, 2001, **101**, 2921–2990.
35 J. Chiefari, Y. K. Chong, F. Ercole, J. Krstina, J. Jeffery, T. P. T. Le, R. T. A. Mayadunne, G. F. Meijs, C. L. Moad, G. Moad, E. Rizzardo and S. H. Thang, *Macromolecules*, 1998, **31**, 5559–5562.
36 C. J. Hawker, A. W. Bosman and E. Harth, *Chem. Rev.*, 2001, **101**, 3661–3688.
37 M. Kamigaito, T. Ando and M. Sawamoto, *Chem. Rev.*, 2001, **101**, 3689–3745.
38 M. Husseman, E. E. Malmström, M. McNamara, M. Mate, D. Mecerreyes, D. G. Benoit, J. L. Hedrick, P. Mansky, E. Huang, T. P. Russell and C. J. Hawker, *Macromolecules*, 1999, **32**, 1424–1431.
39 F. Jasinski, P. B. Zetterlund, A. M. Braun and A. Chemtob, *Prog. Polym. Sci.*, 2018, **84**, 47–88.
40 P. Xiao, J. Zhang, F. Dumur, M. A. Tehfe, F. Morlet-Savary, B. Graff, D. Gigmes, J. P. Fouassier and J. Lalevee, *Prog. Polym. Sci.*, 2015, **41**, 32–66.
41 J.-P. Fouassier and J. Lalevée, in *Photoinitiators*, ed. Wiley, 2021, pp. 35–53.
42 J.-P. Fouassier, D. Burr and F. Wieder, *J. Polym. Sci., Part A: Polym. Chem.*, 1991, **29**, 1319–1327.
43 Y. Shi, G. Liu, H. Gao, L. Lu and Y. Cai, *Macromolecules*, 2009, **42**, 3917–3926.
44 G. W. Sluggett, P. F. McGarry, I. V. Koptyug and N. J. Turro, *J. Am. Chem. Soc.*, 1996, **118**, 7367–7372.
45 C. Decker, *Prog. Polym. Sci.*, 1996, **21**, 593–650.
46 M. Jacobi, *Polym. Paint Color J.*, 1985, **175**, 636.
47 G. W. Sluggett, C. Turro, M. W. George, I. V. Koptyug and N. J. Turro, *J. Am. Chem. Soc.*, 1995, **117**, 5148–5153.
48 J. Tan, H. Sun, M. Yu, B. S. Sumerlin and L. Zhang, *ACS Macro Lett.*, 2015, **4**, 1249–1253.
49 Y. Jiang, N. Xu, J. Han, Q. Yu, L. Guo, P. Gao, X. Lu and Y. Cai, *Polym. Chem.*, 2015, **6**, 4955–4965.
50 J. Tan, D. Liu, Y. Bai, C. Huang, X. Li, J. He, Q. Xu, X. Zhang and L. Zhang, *Polym. Chem.*, 2017, **8**, 1315–1327.
51 T. Majima, W. Schnabel and W. Weber, *Makromol. Chem.*, 1991, **192**, 2307–2315.
52 J. Jakes, *Collect. Czech. Chem. Commun.*, 1995, **60**, 1781–1797.
53 K. Ferji, P. Venturini, F. Cleymand, C. Chassenieux and J.-L. Six, *Polym. Chem.*, 2018, **9**, 2868–2872.
54 P. Lertturongchai, M. I. A. Ibrahim, A. Durand, P. Sunintaboon and K. Ferji, *Macromol. Rapid Commun.*, 2020, **41**, 2000058.
55 D. Ikkene, A. A. Arteni, C. Boulogne, J.-L. Six and K. Ferji, *Macromolecules*, 2022, **55**, 4268–4275.
56 L. P. D. Ratcliffe, A. J. Ryan and S. P. Armes, *Macromolecules*, 2013, **46**, 769–777.
57 A. I. Buzin, M. Pyda, P. Costanzo, K. Matyjaszewski and B. Wunderlich, *Polymer*, 2002, **43**, 5563–5569.
58 D. Ikkene, A. A. Arteni, M. Ouldali, G. Francius, A. Brûlet, J.-L. Six and K. Ferji, *Biomacromolecules*, 2021, **22**, 3128–3137.
59 D. Ikkene, A. A. Arteni, M. Ouldali, J.-L. Six and K. Ferji, *Polym. Chem.*, 2020, **11**, 4729–4740.